[*] Applying Macro Design Tools to the Design of MEMS Accelerometers

[^] Brady R. Davies, M. Steven Rodgers, and Stephen Montague

Intelligent Micromachine Department
Sandia National Laboratories, P.O. Box 5800 MS 1080
Albuquerque, New Mexico 87185-1080
http://www.mdl.sandia.gov/Micromachine

Keywords: accelerometer, silicon micromachining, solid state sensors

ABSTRACT

This paper describes the design of two different surface micromachined (MEMS) accelerometers and the use of design and analysis tools intended for macro sized devices. This work leverages a process for integrating both the micromechanical structures and microelectronics circuitry of a MEMS accelerometer on the same chip. In this process, the mechanical components of the sensor are first fabricated at the bottom of a trench etched into the wafer substrate. The trench is then filled with oxide and sealed to protect the mechanical components during subsequent microelectronics processing. The wafer surface is then planarized in preparation for CMOS processing. Next, the CMOS electronics are fabricated and the mechanical structures are released.

The mechanical structure of each sensor consists of two polysilicon plate masses suspended by multiple springs (cantilevered beam structures) over corresponding polysilicon plates fixed to the substrate to form two parallel plate capacitors. One polysilicon plate mass is suspended using compliant springs forming a variable capacitor. The other polysilicon plate mass is suspended using very stiff springs acting as a fixed capacitor. Acceleration is measured by comparing the variable capacitance with the fixed capacitance during acceleration.

2.0 INTRODUCTION

MicroElectroMechanical Systems (MEMS) technology has tremendous promise and has generated a significant amount of interest in the academic, lab, government, and business sectors. This interest is primarily focused on the perceived potential performance and cost advantages associated with microscale devices fabricated using conventional silicon processing technology and equipment. While the market for micromachined devices is expected to reach between $10[1] billion to $14[2] billion dollars per year by the year 2000, the current and projected market is very segmented. This segmentation phenomenom is also true for the micromachined accelerometer and gyroscope markets. Efficiently and

---

[*] Sandia is a multiprogram laboratory operated by Sandia Corporation, a Lockheed Martin Company, for the United States Department of Energy under Contract DE-AC04-94AL85000.

[^] B.R.D. (correspondence): Email: brdavie@sandia.gov; Telephone: (505) 844-5600
M.S.R. (correspondence): Email: rodgersm@sandia.gov; Telephone: (505) 844-1784
S. M. (correspondence): Email: montags@sandia.gov; Telephone: (505) 844-6954

profitably accessing the various segments of the projected market for micromachined acceleration and rate sensors will likely require significant design flexibility, integration between micromachines and microelectronics, and a full suite of design, simulation, and analysis tools. In order to be profitable, fixed costs associated with developing and maintaining repeatable fabrication processes (equipment, facility, and other process development costs), and the fixed costs associated with designing, analyzing, and laying out micromachines and microelectronics (device development costs), must be shared by several or perhaps many different micromachined accelerometer and gyroscope products.

Various fabrication challenges including layer topography, inter-layer stiction, and residual stress deformation, to name but a few, must be resolved in order to fabricate reliable micromachined accelerometers and other MEMS devices. A description of the processes, design tools, design issues, and example accelerometers follows.

3.0 SURFACE MICROMACHINING FABRICATION PROCESSES

The accelerometers described in this paper were fabricated using processes developed by the author's company. In fact a number of different surface micromachining processes have been developed by the company. Some processes emphasize multiple independent layers of polycrystalline silicon (currently up to five) to enable the development of very mechanically sophisticated devices. Other processes emphasize the integration of micromachine structures with microelectronics to take advantage of performance and cost advantages associated with integration. In general, multi-layer surface micromachining fabrication processes are extremely flexible. They are very flexible because they facilitate significant mechanical design sophistication even though the process steps, material properties, and structural layer spacing are fixed, because the designer has greater latitude to control lateral geometry and greater flexibility to use multiple structural layers than is available in other processes.

3.1 Four-Level Polycrystalline Micromachining Process

In general, micromechanical actuators have not experienced the depth and breadth of development and applications that micromechanical sensors have experienced. Deficiencies in torque and coupling of actuators to other structures were identified as the primary obstacles inhibiting the widespread application of micromechanical actuators. A four-level polycrystalline silicon process was developed to enable fabrication of actuators that were capable of sufficient torque and coupling flexibility to make micromechanical actuators practical[3,4]. The process also enables the development of devices with signficantly greater levels of functionality and flexibility than other comparable processes can provide.

This four-level process includes three movable levels of polysilicon in addition to a stationary level for a total of four levels of polysilicon. These levels are each separated by sacrificial oxide layers. A total of eight mask levels are used in this process. An additional friction-reducing layer of silicon nitride is placed between the layers that form bearing surfaces. The inset (lower right) to Figure 1 illustrates a bearing formed between two layers of mechanical poly. Figure 1 shows two comb-drive actuators driving a set of linkages to a set of rotary gears. This engine can be rotated by applying sinusoidal driving forces 90^{o} out of phase with each other to each of the comb-drive actuators. Operation of the small gears (shown in the inset) at rotational speeds in excess of 300,000 revolutions per minute has

been demonstrated. The operational lifetime of these small devices exceeds $7x10^9$ revolutions. This smaller gear is shown driving a larger (1.6 mm diameter) gear. This larger gear has been driven as fast as 4800 rpm.

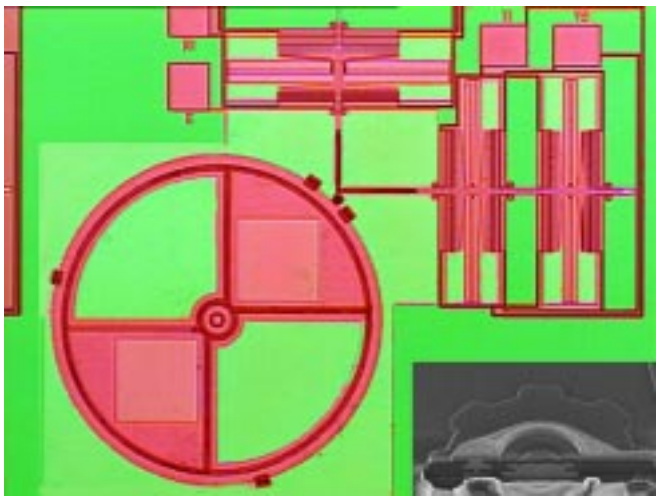

Figure 1. Orthogonal Acting Comb-Drive Actuators

3.2 Integrated Process

A unique micromechanics-first approach has also been developed for on-chip integration of micromechanical structures with CMOS microelectronics[5]. In this approach, micromechanical devices are fabricated in a trench etched in the surface of the wafer. After these devices are complete, the trench is refilled with oxide, planarized using chemical-mechanical polishing, and sealed with a nitride membrane. The wafer with the embedded micromechanical devices is then processed using conventional CMOS processing. Additional steps are added at the end of the CMOS process in order to expose and release the embedded micromechanical devices. The yield of the most recent lots fabricated using this process has exceeded 98% for integrated combustible gas detection systems.

4.0 DESIGN TOOLS

Cost effective MEMS development not only requires reliable and repeatable fabrication processes, but it also requires flexible and integrated design and analysis tools. Several commercial entities have developed design tools for MEMS, each with its unique set of strengths and weaknesses. Additionally, assorted non-MEMS design tools have been applied to design and analysis of MEMS according to the abilities and needs of MEMS designers.

4.1 Mask Layout Tools

The layer geometry (including layers of polycrystalline silicon, silicon dioxide, and silicon nitride) of each patterning step in the fabrication of MEMS devices is defined by a separate 2-D mask. Masks are fabricated from 2-D software drawing files created using a mask layout tool.

Each mask level in the micromachining fabrication process corresponds to one or more mask layout tool drawing layer. Some mask levels correspond to multiple drawing layers in order to simplify the layout

of mask levels. For example, Figure 2 shows a typical set of drawing layers used to define the composite geometry of a structural poly layer. In this example, one layer will be used to define the main structural geometry of a layer (square structure on left), then a second layer will be used to define geometry within the main structural layer to be removed (grid of holes in middle). The two layers are then combined using an XOR (exclusive OR) operation to create a single mask layer geometry definition (right).

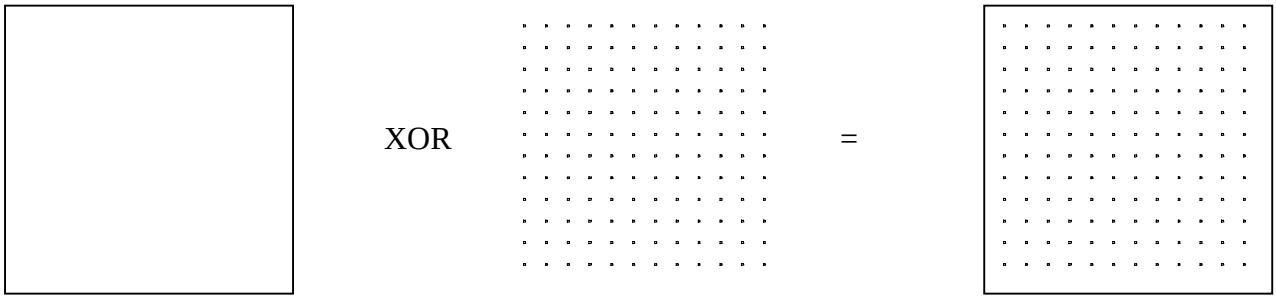

Figure 2: Example XOR Operation

4.2 Mechanical Finite Element Analysis Software

Certain kinds of finite element analysis software can be applied to MEMS devices as long as a good understanding of device and microdomain physics are taken into account and scaling and unit conversion is performed correctly. In the MEMS domain, effects due to Van der Waals forces, capillary and surface tension effects, and electrostatic forces can easily exceed inertial, material deflection, and friction forces which usually dominate models of macrodomain devices. In addition to adapting finite element analysis software that was developed for macroscopic domain devices to microscopic device analysis, several commercial entities are developing analysis software specifically for microscopic devices.

These microdomain specific packages allow the designer to model and analyze a MEMS design with such capabilities as 3-D visualization (automatic construction of a 3-D model of the MEMS device based on the composite of the 2-D mask definitions and the fabrication process description), automatic meshing of the MEMS model (designer defines boundary conditions and external loads then the software automatically creates a finite element mesh of the 3-D model), solver analysis (full model analysis of characteristics such as structural mechanics, electrostatics, vibration, heat transfer, fluid flow, and coupled electro-mechanics), and results visualization or plotting.

4.3 Design Rule Checking Software

Once mask levels have been defined within the drawing tool, certain types of design errors are checked with design rule checking software. Design rule checking (DRC) is the process of checking for violations of design rules for the micromechanical fabrication process. Design rules implemented include minimum feature widths, minimum feature spacing, feature overlap dimensions, etch release hole spacing, etc. Once the device geometry has been defined in the mask layout tool, a device geometry file is created and then translated into a format that can be processed by an integrated circuit layout package that supports DRC for integrated circuits. Special design rules are implemented in the integrated circuit layout package relevant to the design and layout of MEMS structures in the specific surface micromachining process being employed. The DRC capability helps MEMS designers avoid

design mistakes that would jeopardize proper function of their MEMS device (such as not completely separating parts that move relative to each other) or adversely impact other designs on the same wafer (such as not anchoring parts that would float free from one design and mechanically interfere with operation of other designs as shown in Figure 3).

Figure 3: Parts Improperly Anchored

5.0 ACCELEROMETER DESIGN EXAMPLES

Accelerometers are important sensors in a variety of applications ranging from impact sensing and air bag actuation to navigation and flight control. Two such accelerometers were designed at Sandia and will be discussed in the following paragraphs. One accelerometer, which will be refered to as a low-G accelerometer, was designed for fabrication using the four-level polycrystalline silicon process. This accelerometer was designed to measure accelerations between ± 25 G.

The other accelerometer was designed for fabrication using an integrated processe to enable on-chip fabrication of both the mechanical and electronics components of the device. This accelerometer is capable of measuring accelerations exceeding 50,000 G, and will be referred to as a high-G accelerometer. Design of each accelerometer was accomplished using many of the design tools described in this paper.

5.1 Low-G Accelerometer Suspension Design

The low-G accelerometer consists of a plate or proof mass suspended by four folded springs. Above and below the suspended proof mass are an upper and lower electrode, respectively. Each electrode acts as one electrode in a parallel plate capacitor, where the suspended proof mass, which at equilibrium is centered between the upper and lower electrodes, acts as the second parallel plate for both the upper and lower electrodes. Accelerations cause the suspended proof mass to be deflected towards the upper or lower electrode. This changes the capacitance between the upper electrode and the proof mass as well as the capacitance between the lower electrode and the proof mass. This change in capacitance is detected and a voltage is applied to the electrode that the proof mass moving away from. This results in an electrostatic attraction force between the suspended plate mass and the electrode which keeps the proof mass centered between the upper and lower electrode. The voltage (or number of discrete voltage pulses) required to keep the proof mass centered is a measure of acceleration. This type of accelerometer control system was used by Lemkin[6] in the design of a three-axis silicon micromachined accelerometer. This type of control can effectively keep the proof mass stationary with respect to the

upper and lower electrodes resulting in increased linearity and dynamic sensing range of the accelerometer.

The spring suspension system as well as electrostatic electrodes can be seen in this mechanical layout rendering of the accelerometer (Figure 4). Mechanical stops were also implemented at each corner and the center of the capacitive plate sensor to restrict lateral and vertical movement during shock or other high acceleration events.

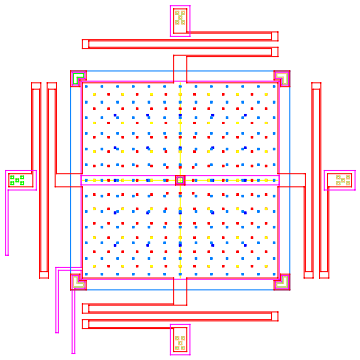

Figure 4: Mechanical Layout Rendering of Low-G Accelerometer Design

5.2 Damping

Damping was estimated by simultaneously applying two different models of squeeze film damping, each of which models some but not all of the applicable characteristics of the suspended mass prototype. (Squeeze-film damping can be defined as the viscous loss of energy due to pumping a viscous fluid out from or into the volume between two moving surfaces.)

The first model[7] is applicable to squeeze-film damping between two parallel disks without perforations that are separated by several μm. In this model, viscous damping occurs due to the movement of fluid around the outside edges of the plates. The damping resistance, R_{film}, is characterized by the following equation (where N-s/m represents the units of Newton-seconds per meter associated with damping resistance):

$$R_{film} = 3\mu S^2/2\pi\delta^3 \quad \text{(N-s/m)} \qquad (1)$$

where μ is the fluid viscosity (18×10^{-6} kg/m-s for air at 20 ºC), S the plate area overlap, and δ the average plate spacing. The second model[7] is applicable to squeeze-film damping when one plate is perforated. In this model, viscous damping occurs due to the flow of fluid through the perforations. The damping resistance, R_{perf}, is characterized by the following equation:

$$R_{perf} = 12\mu G(A)S^2/N\pi\delta^3 \quad \text{(N-s/m)} \qquad (2)$$

where A is the fraction of open area in the plate, and N is the total number of holes in the perforated plate. The function G(A) is described in equation (3).

$$G(A) = [A/2 - A^2/8 - (\ln A)/4 - 3/8] \quad (3)$$

Both models were applied to the design of the suspended mass accelerometer by modeling each of their respective damping contributions and combining them as parallel elements. Additional models can be applied to predict high frequency damping (frequencies greater than 10 kHz).

5.3 Low-G Accelerometer Design Results

The suspended proof mass is perforated by 144, 2µm x 2µm etch-release holes (see Figure 4). The number and spacing of the etch-release holes (necessary for proper fabrication of the sensor element) results in a very low damping ratio (very high Q). The calculated natural frequency of the sensor is 4,070 Hz which is very close to the resonant frequency of 3,898 Hz predicted using the finite element analysis of Table 1. Deflection analysis (Figure 5) predicted maximum deflection of 0.15 µm (in the open loop state) at 10 G of acceleration.

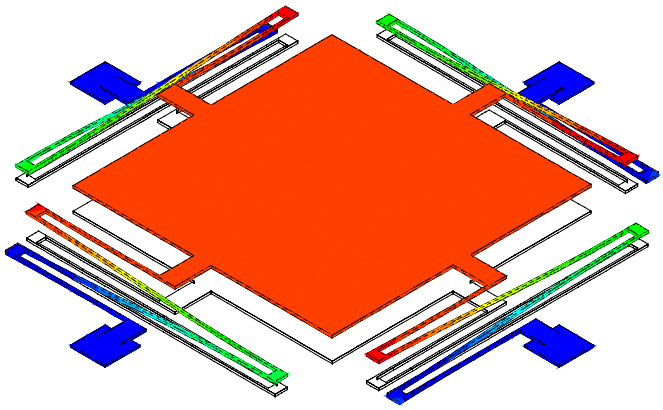

Figure 5: Low G Accelerometer Deflection at 10 G

- Vibration Frequencies:
  - Mode 1: 3,898 Hz
  - Mode 2: 7,008 Hz
  - Mode 3: 7,049 Hz
  - Mode 4: 13,281 Hz
  - Mode 5: 13,573 Hz
  - Mode 6: 19,592 Hz
- Maximum Deflection (@ 10 G):
  - 0.15 µm
- Maximum Stress (@ 10 G):
  - 925 KPa

Table 1: Finite Element Analysis Predictions of Low G Accelerometer

5.4 High-G Accelerometer Suspension Design

A suspended mass, high-G accelerometer was designed and fabricated using an integrated surface-micromachined polysilicon / electronics manufacturing process[3]. This sensor consists of a parallel-plate

capacitor, with one plate stationary with respect to the sensor housing and the second plate suspended by flexible beams that deflect in proportion to the magnitude of the acceleration imposed upon the sensor housing. The sensor was designed to measure accelerations up to 50 kG with a resolution of 50 G.

The mechanical elements of the high-G accelerometer were fabricated using two layers of polycrystalline silicon with a separation of two microns. The upper layer contains the moving mechanical element of the sensor, and the bottom layer acts as both a structural and electrical ground.

The high-G suspended mass sensor consists of twelve bent-beam elements (six on each side) that act as springs to cantilever a 22,600 μm^2 plate mass (top layer of polycrystalline silicon) over a bottom electrode (bottom layer of polycrystalline silicon). A top view of the sensor and reference capacitor is shown in Figure 6. The reference capacitor, on the left, is a parallel plate capacitor identical in geometry to the sensor parallel plate capacitor with the exception of spring elements. Spring elements in the reference capacitor are designed to be very stiff, so that at the acceleration levels relevant to sensor operation, the reference capacitor spring elements permit negligible deflection of the plate mass. The reference capacitance and sensor capacitance are compared electronically to measure acceleration.

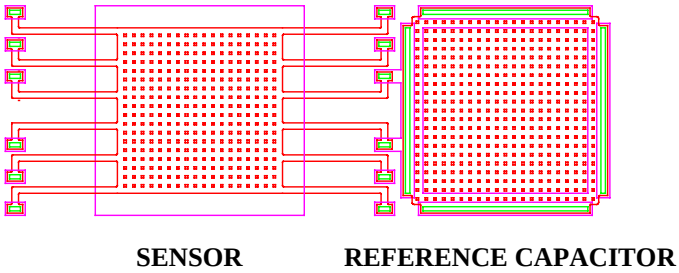

Figure 6: Bent Beam Design for High-G Accelerometer

5.5 High-G Accelerometer Analysis

Results of finite element analysis performed on the high-G accelerometer predicted somewhat different deflection and resonant frequency values than those obtained through manual analysis. The software predicted that the structure would resonate at 151 kHz (Table 2) as compared to the manual analysis prediction of 101 kHz. The finite element software predicted maximum deflection at 50 kG of 0.64 microns (Figure 7) compared to 0.95 microns using manual analysis techniques. Additionally, finite element software predicted a maximum principal stress level of 93.2 MPa (Table 2) at 50 kG compared to 74 MPa using manual analysis techniques.

• Vibration Frequencies: – Mode 1: 151 kHz – Mode 2: 240 kHz – Mode 3: 470 kHz – Mode 4: 498 kHz – Mode 5: 747 kHz – Mode 6: 876 kHz	• Maximum Deflection (@ 50 kG): – 0.64 µm • Maximum Stress (@ 50 kG): – 93.2 MPa

Table 2: Finite Element Analysis Results (at 50 kG)

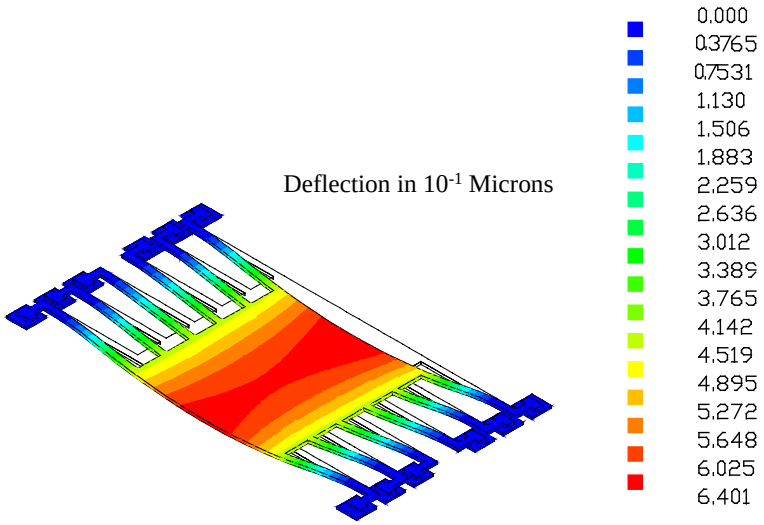

Figure 7: Deflection Analysis of High-G Accelerometer (at 50 kG)

Actual test results for the high-G accelerometer were very positive, with the response of the sensor showing excellent correlation between the shock pulse and sensor output at accelerations up to 50,000 G (actually tested at 46,000 G). Filtered accelerometer response data is shown for a shock pulse of approximately 25 kG in Figure 8 below.

6.0 SUMMARY

The four-level polysilicon fabrication process enables the design and fabrication of force-balanced low-G accelerometers. The integrated process enables the design and fabrication of a high-G accelerometer. Design tools and infrastructure have been developed to support the fabrication of these sophisticated devices. These processes have been used successfully by both internal and external MEMS designers in a wide variety of device applications. Using design tools and process, it is possible to design and fabricate MEMS accelerometers and other devices that work after only one design cycle[8].

ACKNOWLEDGMENTS

The authors wish to express their sincere appreciation to the engineers and technicians who have developed and implemented the processes used in fabricating the micromachines described in this paper. Without the outstanding assistance of these dedicated professionals, the work described above could not have been accomplished.

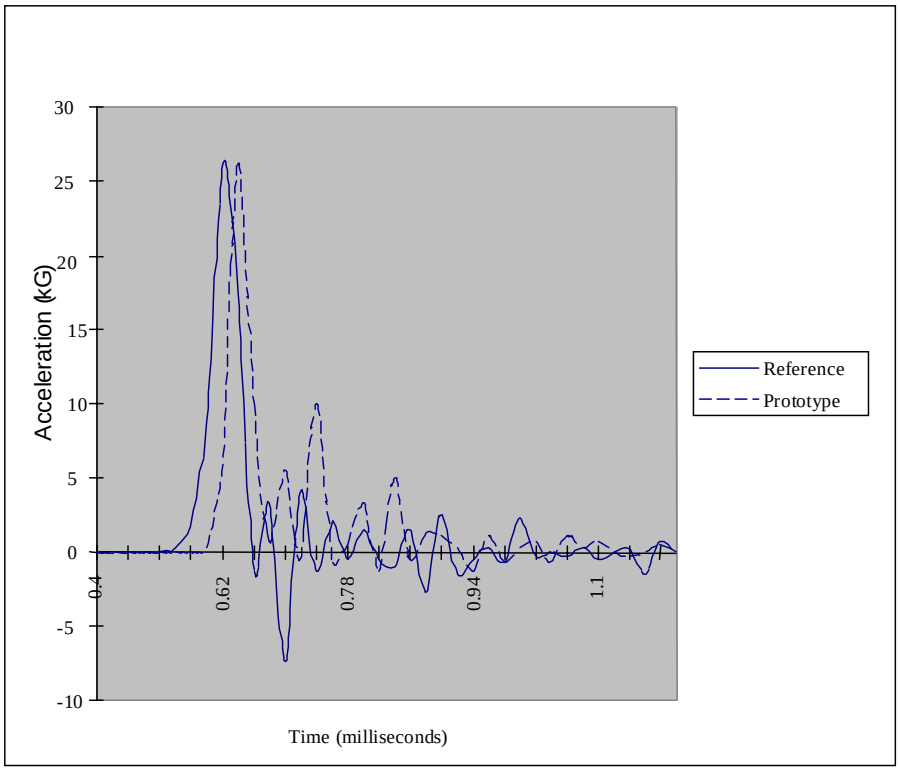

Figure 8: Filtered Acceleration vs. Time plot for Shock Test at 25 kG

REFERENCES

1. S. Marshall, T. Studt, R. Cassidy, "Micromachine sales to grow 50% a year", Micromachine Devices, Vol. 1, No. 1, September 1996.
2. System Planning Corporation, "MicroElectroMechanical Systems (MEMS) – An SPC Market Study", System Planning Corporation, 1994.
3. J. Sniegowski and E. Garcia, "Microfabricated actuators and their applications to optics," *Proceedings of SPIE Photonics West '95*, SPIE,1995.
4. J. Sniegowski and E. Garcia, "Surface-micromachined geartrains driven by an on-chip electrostatic microengine," *IEEE Electron Device Letters*, vol. 17, no. 7, p. 366, 1996.
5. J. Smith, "Micromachined Sensor and Actuator Research at Sandia's Microelectronics Development Laboratory", Invited Presentation, Proc. Sensors Expo Anaheim '96, pp. 119-123, April, 1996.
6. M. A. Lemkin, M. A. Ortiz, N. Wongkomet, B. E. Boser, J. Smith, "A 3-Axis Surface Micromachined ΣΔ Accelerometer", *IEEE International Solid-State Circuits Conference*, pp. 202-203, 1997.
7. T. B. Gabrielson, "Mechanical-Thermal Noise in Micromachined Acoustic and Vibration Sensors", *IEEE Transactions on Electron Devices*, Vol. 40, No. 5, May, 1993.
8. J. H. Comtois, M. Adrian Michalicek, Carole Craig Barron, "Characterization of Electrothermal Actuators and Arrays Fabricated in a Four-Level, Planarized Surface-Micromachined Polycrystalline Silicon Process", *International Conference on Solid-State Sensors and Actuators (Transducers '97*), pp. 769-772, 1997.